Influence of Variations in Imbalanced LISN Termination Impedances on Radiated Emissions

Hossein Rezaei, *Member, IEEE*, Morten Sørensen, *Senior Member, IEEE*, Kim Jensen, *Member, IEEE*, David Pommerenke, *Fellow, IEEE*, and Daryl G. Beetner, *Fellow, IEEE*

***Abstract*— Radiated emissions measurements are often performed using a line impedance stabilization network (LISN) with a balanced termination, but in the real world, the common-mode characteristic of the termination may be highly variable. An asymmetric LISN allows testing under more realistic asymmetric termination conditions. The common-mode termination impedance of these LISNs must fall within set tolerances, but the impact of these tolerances is unknown. An analysis of the radiated emissions from a device under test (DUT) for a wide variety of power cable termination impedances is performed in the following paper to estimate the impact of allowed variations in imbalanced LISN termination impedances on the uncertainty or radiated emissions measurement. Methods are developed to rapidly predict emissions by first determining the *S*-parameters between ports located at the DUT, at the power cable termination, and at a "port" measuring radiated emissions. The *S*-parameters are then used in analytical equations to predict the radiated emissions for a variety of termination impedances and the variation in radiated emissions caused by the allowed variation in asymmetric LISN termination impedances. Results demonstrate that previous recommendations allowing a ±30° change in the phase and ±10% change in the magnitude of the asymmetric LISN termination create about 5 dB maximum variation in radiated emission from 30 to 300 MHz among the tested configurations. According to the model used in this article, the expanded standard uncertainty in the emissions measurements resulting from these variations is about 9.8 dB, which is well below the 15.5 dB limit suggested by CISPR 16-4-1.**

***Index Terms*— Line impedance stabilization network (LISN), Mason's rule, radiated emissions, signal flow graph, termination impedance.**

I. Introduction

THE geometry of a test setup, the termination impedances used in the setup, and the chamber performance can all influence the radiated emissions measured for a device under test (DUT) [1], [2], [3]. In helping to limit variability in results with termination impedance, emission measurements are often made using a line impedance stabilization network (LISN) or a coupling/decoupling network for ac mains (CDNE-M) to terminate the power lines, although neither of these is purely resistive over the working bandwidth and may exhibit some change in magnitude and phase [1], [2], [3]. The results of round-robin testing for radiated emissions show that using a balanced LISN will improve the reproducibility of the radiated emission measurement as the average emissions differ by only 4 dB; however, those variations in measurements were as large as +18/−10 dB without a LISN [4], [5], [6]. Additionally, radiated emission measurements from different studied cases verified that the LISN makes the test results closer to the true radiation from the DUT [7], [8]. Reasonable variations in the magnitude and phase of the LISN impedance, however, can significantly alter the measurement of radiated emissions [9]. Importantly, the limited variation in termination impedances with a traditional symmetric LISN may not adequately capture the variation in impedances—and of the radiated emissions—seen in the real world [10], [11], [12], [13]. An asymmetric LISN can improve the capture of real-world emissions by allowing for differential-to-common mode conversion of power-line signals [10], [11], [12], [13]. The impact of standard, acceptable variations in the termination impedances on the radiated emissions is, however, not well defined. A method to rapidly evaluate the impact of variations in the LISN termination impedances is developed in the following paper and is used to quantify their impact on the variability of radiated emissions measurements.

The standard compliance uncertainty (SCU) is used to evaluate the impact of the complex termination of the LISN on the radiated emissions test result. The SCU is often used in EMC standards and characterizes "the uncertainty associated with the statement that a given product complies with the requirements specified in a CISPR recommendation" [14]. CISPR 16-4-1 suggests 15.5 dB as an allowable SCU [9], [14] and includes variations from the termination impedance as well as the operating state of the equipment under test (EUT), the cable arrangement, the instrumentation and measurement uncertainty. The SCU arising from the termination impedances should be well below this 15.5 dB limit.

The impact of variations in termination impedance on radiated emissions was studied in [9] for a three-wire symmetric VHF-LISN with a 50 Ω termination of each line. The impact of a variation in the magnitude (±10 Ω variation) and

Received 16 November 2023; revised 7 January 2024; accepted 15 January 2024. Date of publication 18 November 2024; date of current version 4 December 2024. This work was supported by the National Science Foundation under Grant IIP-1916535. The Associate Editor coordinating the review process was Dr. Yang Bai. *(Corresponding author: Hossein Rezaei.)*

Hossein Rezaei is with Solidigm Technology, Rancho Cordova, CA 95670 USA (e-mail: hossein.rezaei@ieee.org).

Morten Sørensen is with the Department of Engineering and Test, FORCE Technology, 8220 Aarhus, Denmark (e-mail: moso@forcetechnology.com).

Kim Jensen is with Grundfos Holding A/S, 8850 Bjerringbro, Denmark (e-mail: kimjensen@grundfos.com).

David Pommerenke is with the Institute of Electronics, Graz University of Technology, 8010 Graz, Austria, also with Silicon Austria Labs, 8010 Graz, Austria, and also with Graz EMC Laboratory, Graz University of Technology, 8010 Graz, Austria (e-mail: david.pommerenke@tugraz.at).

Daryl G. Beetner is with the EMC Laboratory, Missouri University of Science and Technology, Rolla, MO 65409 USA (e-mail: daryl@mst.edu).

Digital Object Identifier 10.1109/TIM.2024.3500049

phase (±25° variation) was considered over a frequency range from 30 to 300 MHz. For decreasing simulation time, only 99 different terminations were considered. Radiated emissions were resimulated for the entire structure for each of the 99 terminations. By using this approach the authors were able to determine an acceptable tolerance for the magnitude and phase of the terminating impedances. It is notable that while 99 combinations are numerous and take a long time to simulate, there were also large "holes" in the Smith chart of this study, so that the study may miss a worst case.

To the best of our knowledge, no one has addressed the impact of LISN tolerances on the uncertainty in radiated emissions measurements, particularly for an asymmetric VHF LISN [13]. The working group in [10] proposed that the magnitude of the termination impedance for an asymmetric VHF LISN could vary by ±10%, and in [13], it was proposed that the phase could also vary by ±30°, but no deep analysis of this variation has been performed. In the following work, we develop a fast simulation method to investigate the impact of variations in imbalanced termination impedances of an asymmetric VHF LISN on radiated emissions. In the proposed approach, a 3-D electromagnetic simulation is performed once, and then radiated emissions are estimated for a variety of terminations on the Smith chart using the *S*-parameters from the full-wave simulation while sweeping magnitude and phase in a postprocessing step. Radiated emissions are calculated analytically using *S*-parameters between the DUT, the power cable termination at the LISN, and their relationship to the radiated emissions as found from the simulation. This method reduces the number of full-wave simulations and makes a parametric sweep of the complex termination impedance possible. These results are then used to estimate the SCU in the radiated emissions measurements.

This article is organized as follows. Development of the simulation model and the formulas required to estimate radiated emissions analytically in postprocessing are shown in Section II, where equations for emissions are also developed for a simple one-wire setup and for imbalanced setups with two-wire and three-wire terminations. These equations are validated in Section III and are used to study the measurement uncertainty in radiated emissions caused by variable termination conditions. The impact of these terminations on the SCU is analyzed in Section IV. Conclusions are provided in Section V. It should be noted that this article reuses some content from the Author's PhD dissertation [15] in all sections with permission.

II. Construction of the Postprocessing Method

The DUT used in this study was a solid metal box with dimensions 0.3 × 0.3 × 0.1 m located 0.8 m above an infinite ground plane, as shown in Fig. 1(a) [6], [13].

A 1.5-m power cable was connected to the box and terminated to an infinite return plane. The wire was connected to the DUT using different excitations, e.g., CM and DM sources providing 1 V with a 50 Ω output impedance (i.e., using an *S*-parameter excitation). A low-impedance (10 Ω) source was selected to connect the wires to the DUT, as this is similar to a poor shield connection and causes similar voltage drops [13].

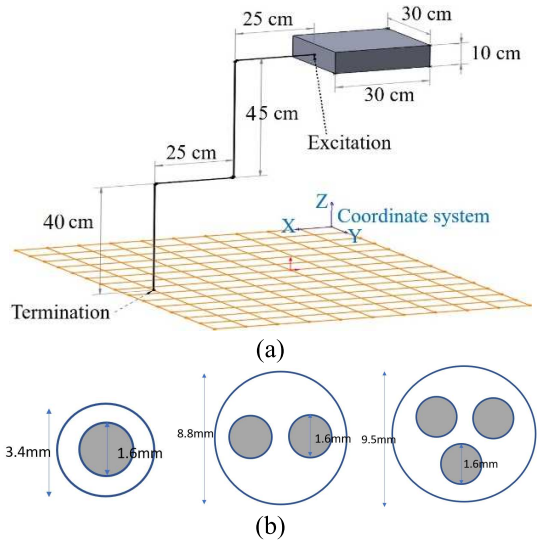

Fig. 1. Three-dimensional full-wave simulation setup for one-wire application [13]. (a) Simulation setup and (b) cross section of one-wire, two-wire, and three-wire PVC cables. Far-field emissions were measured on a sphere 3 m from the DUT.

TABLE I
CST Setting for Full-Wave Simulation

CST Setting	Explanation
Frequency	0-300 MHz
Background	Normal
Boundaries	Open (add space) in all directions except at Ymin (Et = 0)
Field Monitor	Farfield / RCS, Transient Broadband
Setup Solver	Time Domain Solver
Post Processing	E-field, 3D, radiated emission at every 5° in azimuth and elevation on a sphere 3 m from the DUT
Maximum cells per wavelength	40
Maximum cell per max model box edge	40
Fraction of maximum cell near to model	35

The connection of these ports between power lines will be discussed later in this section. The termination impedances were set to mimic those of a VHF LISN [10], [11], [12], [13]. Three-dimensional full wave simulations were performed on this structure using the finite integration technique solver in CST [16]. The settings for this simulation are summarized in Table I. Radiated emissions were found in a postprocessing step using a MATLAB [17] code written by the authors. This postprocessing step allows the incorporation of a variety of passive complex termination impedances when finding the emissions.

Three power cord geometries were studied, including a one-wire, two-wire, or three-wire cord [Fig. 1(b)]. Each wire in the cables had a diameter of 1.62 mm and was covered with PVC insulation (0.89 mm thickness) with a relative permittivity of 4, relative permeability of 1, and loss tangent of 0.06. The distance between the wires was 2.35 mm. The cable jacket had a diameter of 9.5 mm, also made from PVC. It should be noted that the mode conversion in the cable can be modified

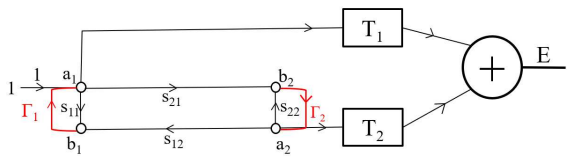

Fig. 2. Signal flow graph for a two-port system generating radiated emissions.

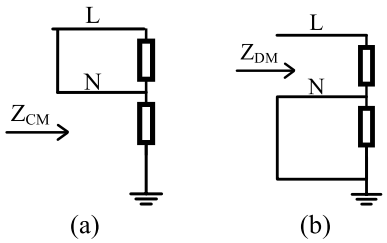

Fig. 3. Schematic of two-wire imbalanced termination. (a) Z_{CM} and (b) Z_{DM}.

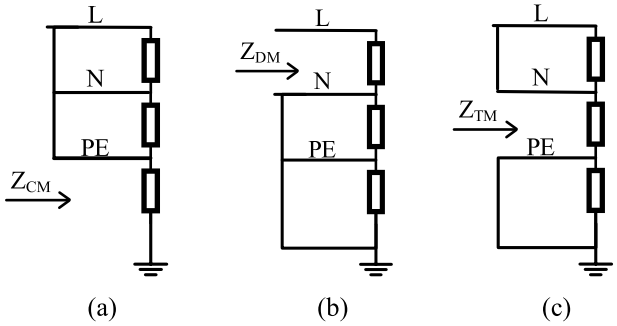

Fig. 4. Schematic of three-wire imbalanced termination. (a) Z_{CM}, (b) Z_{DM}, and (c) Z_{TM}.

by changing the cable height and the bends in the cable. Here, we aim to study the effect of variable termination impedance for radiated emissions for a set of fixed example geometries. For a new geometry, one needs to run only one full-wave simulation to find the transfer functions and then determine the impact of terminations in postprocessing analyses.

The "one-wire" configuration shown in Fig. 1 can be excited from two locations, on both the excitation and termination side of the wire (as shown). This structure can be modeled as a two ports network with a signal flow graph as shown in Fig. 2, where a_1 and b_1 represent the forward and backward propagating waveforms at the excitation port (port 1, excited by a 1 V source), a_2 and b_2 represent the termination port (port 2), T_1 and T_2 are the transfer functions from the forward propagating waves a_1 and a_2, respectively, to the radiated E-field at a particular location, and Γ_1 and Γ_2 are the reflection coefficients at each port. The radiated E-field is the superposition of the quantity coming from T_1 and T_2. For an isotropic antenna, the radiated power density at a distance R is [18]

$$S(\theta,\phi,r)=\frac{P_{\text{rad}}}{4\pi r^2}=\frac{P_{\text{fwd}}G_{\text{re}}(\theta,\phi)}{4\pi r^2} \tag{1}$$

where P_{fwd} is the forward power. The radiated E-field at a distance R can then be found as [18]

$$E(\theta,\phi,r)=\sqrt{\frac{P_{\text{fwd}}G_{\text{re}}(\theta,\phi)}{4\pi r^2}Z_s} \tag{2}$$

where Z_s is the free space wave impedance. The complex transfer function T can then be calculated as

$$T(\theta,\phi,r)=\frac{E(\theta,\phi,r)}{\sqrt{P_{\text{fwd}}}}=\sqrt{\frac{G_{\text{re}}(\theta,\phi)}{4\pi r^2}Z_s} \tag{3}$$

where $\sqrt{P}_{\text{fwd}}$ is the forward wave as in the signal flow graph. For any point in space in the full wave simulation, the electrical field strength can be exported and normalized with the forward wave in CST [16] as

$$E(\theta,\phi,r)_i=\left(\sqrt{P}_{\text{fwd}}\right)_i T(\theta,\phi,r)_i=A_i T(\theta,\phi,r)_i \tag{4}$$

where i represents the port number at the location where the transfer parameter T_i is found.

The signal flow graph can be used to find an analytical solution for radiated emissions with different termination impedances by applying Mason's rule [19]. By using this rule, the total electric field (E) resulting from a 1 V stimulation at the excitation port is given by

$$E(r,\theta,\varphi)=\frac{1-S_{22}\Gamma_2}{D}T_1(r,\theta,\varphi)+\frac{S_{21}\Gamma_2}{D}T_2(r,\theta,\varphi) \tag{5}$$

$$D=1-S_{11}\Gamma_1-S_{22}\Gamma_2-S_{12}S_{21}\Gamma_1\Gamma_2+S_{11}\Gamma_1S_{22}\Gamma_2. \tag{6}$$

For determining the S-parameters for this equation, the setup shown in Fig. 1 should be created in a full-wave tool and be excited with S-parameter ports from two locations on both the excitation and termination side of the wire [Fig. 1(a)]. In our case, the transfer functions (T) are created from the far-field radiated emission results at points distributed every 5° in azimuth and elevation on a 3-m radius sphere centered around the DUT. These S-parameter results are then exported and used to calculate the maximum radiated emissions from the DUT with (5). It is also possible to obtain the electric field on a cylindrical surface as it is specified in CISPR.

While a symmetric two-wire or three-wire 50 Ω termination was studied as in [1] and [10], any termination could be used. Here, we use an approach as in (5) to investigate the effects of variable complex impedance terminations on the radiated emissions for an imbalanced two-wire or three-wire termination (Figs. 3 and 4) [11], [12], [13], [20]. Although the magnitude and phase of the imbalanced termination have not yet been standardized, it is worthwhile to investigate the variation caused by the imbalanced termination since it reflects the impedances in a typical household better than is realized with a symmetric termination [13]. The magnitude and phase of the termination impedances studied here are summarized in Figs. 3 and 4 are as follows.

1) *In Two-Wire Applications:*
   a) Common mode impedance = 150 Ω ± 10% (±30° in phase) @ 30∼300 MHz. This is the impedance of two wires (L shorted to N) referenced to the ground-plane [Fig. 3(a)].
   b) Differential mode impedance = 100 Ω ± 10% (±30° in phase) @ 30∼300 MHz. This is defined as the impedance of L to N while N is shorted to the ground plane [Fig. 3(b)].

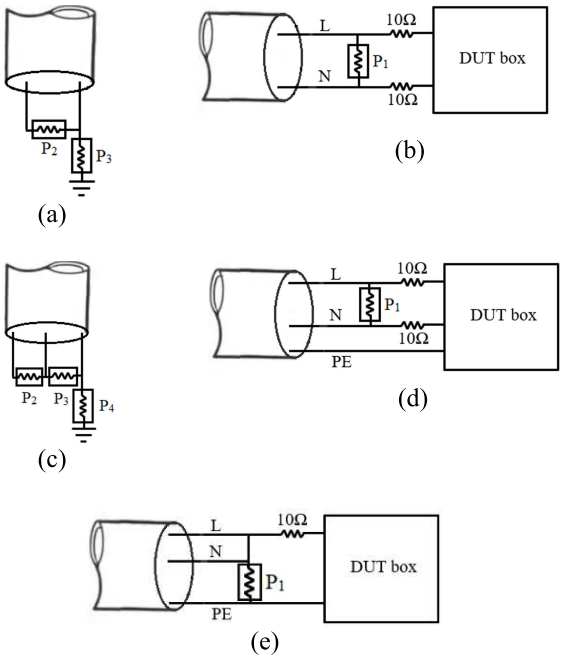

Fig. 5. Connections used in the 3-D full-wave simulation setup. (a) Two-wire imbalanced termination, (b) differential-mode excitation of two-wire setup, (c) three-wire imbalanced termination, (d) differential-mode excitation of three-wire setup, and (e) tertiary-mode excitation for three-wire setup [13].

2) *In Three-Wire Applications:*

a) Common mode impedance = 90 Ω ± 10% (±30° in phase) @ 30∼300 MHz. This is the impedance of (*L* shorted to *N* shorted to protective earth (PE) to the ground plane [Fig. 4(a)].

b) Differential mode impedance = 100 Ω ± 10% (±30° in phase) @ 30∼300 MHz, which is defined as the impedance of *L* to (*N* shorted to PE shorted to the ground plane) [Fig. 4(b)].

c) Tertiary mode impedance = 60 Ω ± 10% (±30° in phase) @ 30∼300 MHz. As shown in Fig. 4(c), this is defined as the impedance of (*L* shorted to *N*) to (PE shorted to ground plane).

Fig. 5 shows the excitation and termination sides for the two-wire and three-wire setups (with termination impedances represented as ports). Fig. 5(b) and (d) show differential-mode excitation of the two-wire and three-wire setups, respectively. Some products have a dominant common mode on the Line (*L*) and Neutral (*N*) with respect to the PE line. This is called "tertiary-mode excitation" [13] which is represented in Fig. 5(e). The termination sides of the two-wire and three-wire imbalanced LISN are shown in Fig. 5(a) and (c), respectively. The device with imbalanced termination converts differential-mode current to common-mode current that can increase radiated emissions. The differential-mode to common-mode conversion is defined as the ratio of the differential mode power that is returned along the cable toward the DUT in common mode [13]. The conversion is expressed with the reflection at ports 2, 3, and 4 (Fig. 5).

The two-wire and three-wire setups shown in Fig. 5 can be represented using three or four S-parameter sources, respectively. The ports were used to excite the structure from both sides of the wire to determine the transfer functions (T) from the ports to the radiated fields. The two-wire structure shown in Fig. 5(a) and (b) was modeled as a three ports network with the signal flow graph shown in Fig. 6. The three-wire termination in Fig. 5(c), with the excitation shown in either Fig. 5(d) or Fig. 5(e), was modeled as a four-port network, as shown in Fig. 7. As in Fig. 2, the forward and backward propagating waves associated with port i are denoted by nodes a_i and b_i in these graphs. Once the S-parameters were found for each configuration, ports 2, 3, and 4 in Figs. 6 and 7 were replaced with two-wire or three-wire imbalanced terminations (Figs. 3 and 4) and the reflection coefficients were calculated for each impedance. Throughout this article, port 1 corresponds to a_1–b_1 (Figs. 5–7), port 2 corresponds to a_2–b_2 (Figs. 5–7), Port3 corresponds to a_3–b_3 (Figs. 5–7) and port 4 corresponds to a_4–b_4 (Figs. 5 and 7).

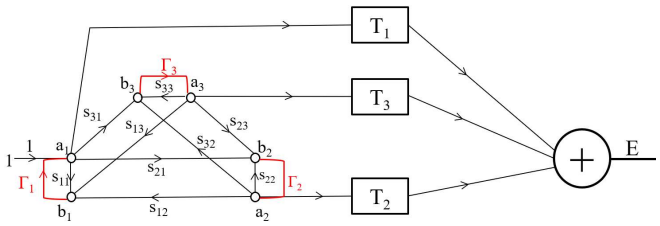

Fig. 6. Signal flow graph for the two-wire, three-port network, excited by a 1 V source.

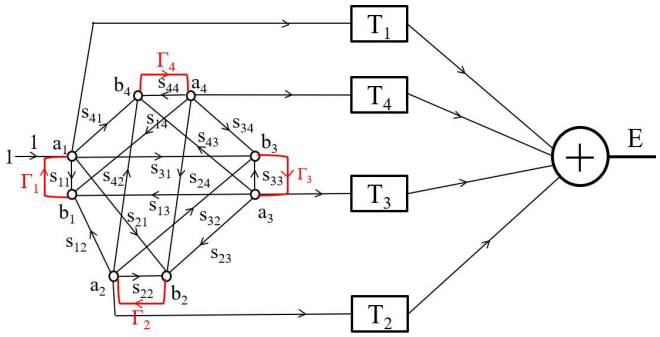

Fig. 7. Signal flow graph for the three-wire, four-port network, excited by a 1 V source.

Mason's rule was applied to the signal flow graph in Fig. 6 to find an analytical formula for the radiated field as

$$E(r,\theta,\varphi) = \frac{F_1}{D}T_1(r,\theta,\varphi) + \frac{F_2}{D}T_2(r,\theta,\varphi) + \frac{F_3}{D}T_3(r,\theta,\varphi) \quad (7)$$

$$D = 1 - (S_{11}\Gamma_1 + S_{22}\Gamma_2 + S_{33}\Gamma_3 + S_{12}S_{21}\Gamma_1\Gamma_2 + S_{13}S_{31}\Gamma_1\Gamma_3 + S_{23}S_{32}\Gamma_2\Gamma_3) + S_{11}S_{22}\Gamma_1\Gamma_2 + S_{11}S_{33}\Gamma_1\Gamma_3 + S_{22}S_{33}\Gamma_2\Gamma_3 \quad (8)$$

$$F_1 = 1 - (S_{22}\Gamma_2 + S_{33}\Gamma_3 + S_{23}S_{32}\Gamma_2\Gamma_3) + S_{22}S_{33}\Gamma_2\Gamma_3 \quad (9)$$

$$F_2 = (1 - S_{33}\Gamma_3)S_{21}\Gamma_2 + S_{31}S_{23}\Gamma_2\Gamma_3 \quad (10)$$

$$F_3 = (1 - S_{22}\Gamma_2)S_{31}\Gamma_3 + S_{21}S_{32}\Gamma_2\Gamma_3 \quad (11)$$

where $E(r,\theta,\varphi)$ is the radiated emissions at a point on a 3-m radius sphere, Γ_2 and Γ_3 are reflection coefficients related to the imbalanced termination impedances at ports 2 and 3, Z_{DM}

and Z_{CM} (Fig. 3), respectively, and $T_1(r,\theta,\varphi)$, $T_2(r,\theta,\varphi)$, and $T_3(r,\theta,\varphi)$ are the transfer coefficients to the field point corresponding to excitations at each port in the full-wave solver. By applying Mason's rule to the three-wire setup in Fig. 7, the radiated emissions can be found to be

$$E(r,\theta,\varphi) = \frac{F_1}{D}T_1(r,\theta,\varphi) + \frac{F_2}{D}T_2(r,\theta,\varphi) + \frac{F_3}{D}T_3(r,\theta,\varphi) + \frac{F_4}{D}T_4(r,\theta,\varphi) \quad (12)$$

$$\begin{aligned} D = 1 &- (S_{11}\Gamma_1 + S_{22}\Gamma_2 + S_{33}\Gamma_3 \\ &+ S_{44}\Gamma_4 + S_{12}S_{21}\Gamma_1\Gamma_2 + S_{13}S_{31}\Gamma_1\Gamma_3 \\ &+ S_{14}S_{41}\Gamma_1\Gamma_4 + S_{23}S_{32}\Gamma_2\Gamma_3 \\ &+ S_{24}S_{42}\Gamma_2\Gamma_4 + S_{34}S_{43}\Gamma_3\Gamma_4 \\ &+ S_{23}S_{34}S_{42}\Gamma_2\Gamma_3\Gamma_4 + S_{43}S_{32}S_{24}\Gamma_2\Gamma_3\Gamma_4) \\ &+ S_{11}S_{22}\Gamma_1\Gamma_2 + S_{11}S_{33}\Gamma_1\Gamma_3 + S_{11}S_{44}\Gamma_1\Gamma_4 \\ &+ S_{22}S_{33}\Gamma_2\Gamma_3 + S_{22}S_{44}\Gamma_2\Gamma_4 + S_{33}S_{44}\Gamma_3\Gamma_4 \\ &+ S_{43}S_{34}S_{11}\Gamma_1\Gamma_3\Gamma_4 + S_{23}S_{32}S_{11}\Gamma_1\Gamma_2\Gamma_3 \\ &+ S_{24}S_{42}S_{11}\Gamma_1\Gamma_2\Gamma_4 + S_{43}S_{34}S_{22}\Gamma_2\Gamma_3\Gamma_4 \\ &+ S_{13}S_{31}S_{22}\Gamma_2\Gamma_3\Gamma_1 + S_{14}S_{41}S_{22}\Gamma_2\Gamma_4\Gamma_1 \\ &+ S_{14}S_{41}S_{33}\Gamma_1\Gamma_3\Gamma_4 + S_{42}S_{24}S_{33}\Gamma_2\Gamma_3\Gamma_4 \\ &+ S_{12}S_{21}S_{33}\Gamma_1\Gamma_2\Gamma_3 + S_{12}S_{21}S_{44}\Gamma_1\Gamma_2\Gamma_4 \\ &+ S_{13}S_{31}S_{44}\Gamma_1\Gamma_3\Gamma_4 + S_{23}S_{32}S_{44}\Gamma_2\Gamma_3\Gamma_4 \\ &- S_{11}S_{22}S_{33}\Gamma_1\Gamma_2\Gamma_3 - S_{11}S_{33}S_{44}\Gamma_1\Gamma_3\Gamma_4 \\ &- S_{22}S_{33}S_{44}\Gamma_2\Gamma_3\Gamma_4 - S_{11}S_{22}S_{44}\Gamma_1\Gamma_2\Gamma_4 \end{aligned} \quad (13)$$

$$\begin{aligned} F_1 = 1 &- (S_{22}\Gamma_2 + S_{33}\Gamma_3 + S_{44}\Gamma_4 + S_{23}S_{32}\Gamma_2\Gamma_3 \\ &+ S_{24}S_{42}\Gamma_2\Gamma_4 + S_{34}S_{43}\Gamma_3\Gamma_4 \\ &+ S_{23}S_{34}S_{42}\Gamma_2\Gamma_3\Gamma_4 + S_{43}S_{32}S_{24}\Gamma_2\Gamma_3\Gamma_4) \\ &+ S_{22}S_{33}\Gamma_2\Gamma_3 + S_{22}S_{44}\Gamma_2\Gamma_4 \\ &+ S_{33}S_{44}\Gamma_3\Gamma_4 + S_{43}S_{34}S_{22}\Gamma_2\Gamma_3\Gamma_4 \\ &+ S_{42}S_{24}S_{33}\Gamma_2\Gamma_3\Gamma_4 \\ &+ S_{23}S_{32}S_{44}\Gamma_2\Gamma_3\Gamma_4 - S_{22}S_{33}S_{44}\Gamma_2\Gamma_3\Gamma_4 \end{aligned} \quad (14)$$

$$\begin{aligned} F_2 = (1 &- S_{33}\Gamma_3 - S_{44}\Gamma_4 - S_{34}S_{43}\Gamma_3\Gamma_4 \\ &+ S_{33}S_{44}\Gamma_3\Gamma_4)S_{21}\Gamma_2 + S_{31}S_{23}\Gamma_2\Gamma_3(1 - S_{44}\Gamma_4) \\ &+ S_{41}S_{24}\Gamma_2\Gamma_4(1 - S_{33}\Gamma_3) + S_{41}S_{34}S_{23}\Gamma_2\Gamma_3\Gamma_4 \\ &+ S_{31}S_{43}S_{24}\Gamma_2\Gamma_3\Gamma_4 \end{aligned} \quad (15)$$

$$\begin{aligned} F_3 = (1 &- S_{22}\Gamma_2 - S_{44}\Gamma_4 - S_{24}S_{42}\Gamma_2\Gamma_4 \\ &+ S_{22}S_{44}\Gamma_2\Gamma_4)S_{31}\Gamma_3 + S_{21}S_{32}\Gamma_2\Gamma_3(1 - S_{44}\Gamma_4) \\ &+ S_{41}S_{34}\Gamma_3\Gamma_4(1 - S_{22}\Gamma_2) \\ &+ S_{41}S_{24}S_{32}\Gamma_2\Gamma_3\Gamma_4 + S_{21}S_{42}S_{34}\Gamma_2\Gamma_3\Gamma_4 \end{aligned} \quad (16)$$

$$\begin{aligned} F_4 = (1 &- S_{22}\Gamma_2 - S_{33}\Gamma_3 - S_{23}S_{32}\Gamma_2\Gamma_3 \\ &+ S_{22}S_{33}\Gamma_2\Gamma_3)S_{41}\Gamma_4 + S_{21}S_{42}\Gamma_2\Gamma_4(1 - S_{33}\Gamma_3) \\ &+ S_{31}S_{43}\Gamma_3\Gamma_4(1 - S_{22}\Gamma_2) + S_{21}S_{43}S_{32}\Gamma_2\Gamma_3\Gamma_4 \\ &+ S_{31}S_{23}S_{42}\Gamma_2\Gamma_3\Gamma_4 \end{aligned} \quad (17)$$

where Γ_1, is the reflection coefficient at the excitation source, and Γ_2, Γ_3, and Γ_4 are the reflection coefficients at ports 2, 3, and 4, related to Z_{DM}, Z_{TM}, and Z_{CM} in Fig. 4, respectively. T_i is the transfer function from node a_i to the radiated emissions $E(r,\theta,\varphi)$ at a point on 3-m radius sphere.

III. Validation and Application of the Postprocessing Method

To verify the method, two simulations were performed in the full-wave solver for each setup. First, all three setups were simulated with a series *RLC* lumped element impedance connected across the terminations between the cable and the return plane. Field monitors were used to find the radiated emissions at different frequencies at points across a 3-m radius sphere surrounding the DUT. The maximum radiated emissions were found as a function of frequency and used to evaluate the accuracy of the equations shown in (1)–(3) when they were used to find the emissions.

Second, each S-parameter port was excited separately in the full-wave solver to find the transfer functions T_1 through T_4 (Figs. 2, 6, and 7) between each port and the radiated fields at each evaluated location (every 5° in azimuth and elevation) on the sphere. The reflection coefficients for the *RLC* impedance used in step one were then found using the signal flow graphs in Figs. 2, 6, and 7. For example, if the source is driving a 50 Ω port 1 in Figs. 6 and 7 the input reflection coefficient (Γ_1) will be zero. The reflection coefficient for an ideal 150 Ω termination [21], [22] in the one-wire setup (Fig. 2) is

$$\Gamma_2 = \frac{Z_L - 50}{Z_L + 50}_{Z_L = 150\,\Omega} = 0.5 \quad (18)$$

giving the following equation for the radiated electric field:

$$E(r,\theta,\varphi) = T_1(r,\theta,\varphi) + \frac{0.5 * S_{21}}{1 - 0.5 * S_{22}}T_2(r,\theta,\varphi). \quad (19)$$

The equivalent reflection coefficient can be calculated in the same way for the terminations in the two or three- wire setups (Figs. 6 and 7). The radiated emissions were then calculated using (5)–(17) for the three different setups. The technique will be validated for each set-up in Sections III-A–III-C. Once validated, it will be used to determine the impact of variations in the phase and magnitude of the termination impedance on radiated emissions. It is worth mentioning that beyond the initial set of simulations required to find the S-parameters and transfer coefficients, no additional full-wave simulations are required. Radiated emissions can be found easily by updating the reflection coefficients for an arbitrary termination.

A. One-Wire Setup

The analysis of the one-wire setup was performed with the setup shown in Fig. 1, which is terminated to the ground plane with the series *RLC* combination: $R = 135\ \Omega$, $L = 10$ nH, and $C = 70$ pF. The *RLC* terminations were selected to have a worst-case variation of up to 30° variation on phase plus a 10% change in the magnitude. The specific values of resistance, capacitance, and inductance were chosen based on the measured values that were observed in a VHF LISN in [13].

As shown in Fig. 8, there was less than a 0.3 dB difference from 30 to 300 MHz between the full-wave simulation including the terminations and the values calculated using (5). This comparison shows a good agreement between two methods for different source impedances other than 50 Ω and verifies

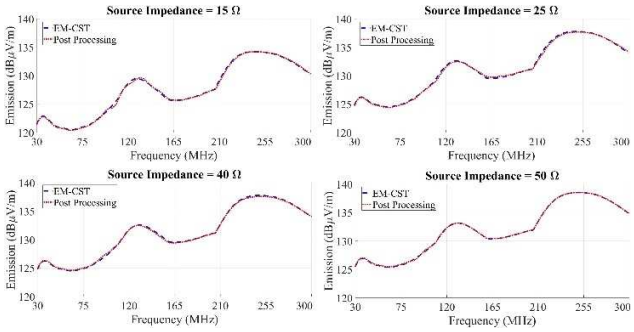

Fig. 8. Radiated emissions from the one-wire setup with the series *RLC* combination $R = 135\ \Omega$, $L = 10$ nH, and $C = 70$ pF.

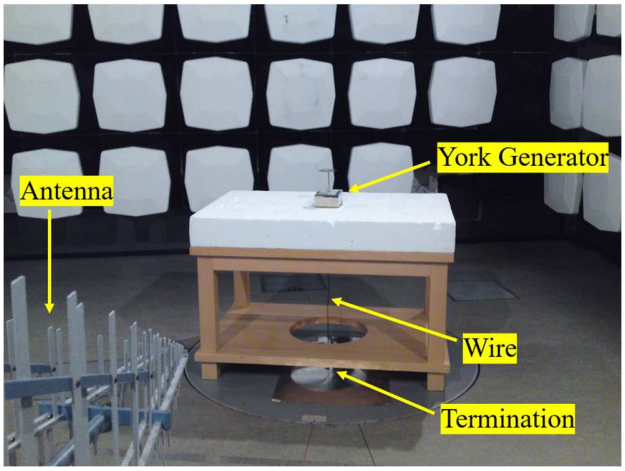

Fig. 9. Measurement setup with York Generator.

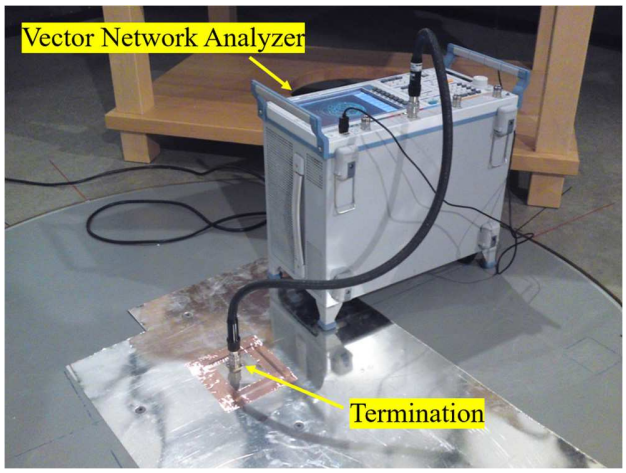

Fig. 10. Measurement setup of a load with vector network analyzer.

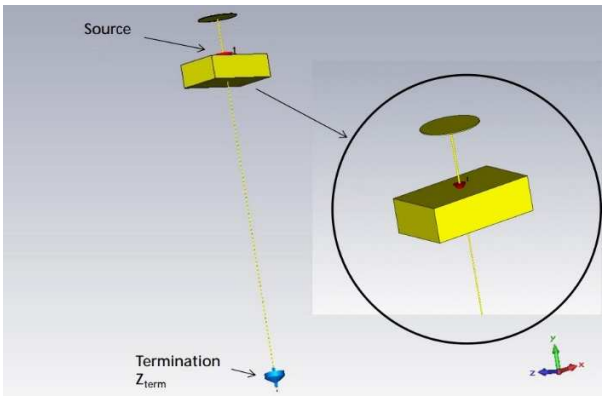

Fig. 11. Three-dimensional full-wave simulation setup with York Generator.

that the postprocessing step reproduces the results from 3-D full-wave simulation well.

The simulation model and postprocessing methodology used with the one-wire setup was validated experimentally. A York Generator [23] was mounted on the table (located 0.8 m above the ground plane), and the termination cable was connected to the floor (Fig. 9). The York Generator was connected to the inner pin of the *N*-Connector. Radiated emissions were captured with different loads and compared with the simulation results. For more accurate simulation results, different loads were measured using a R&S[1]ZNB4 Vector Network Analyzer [24] and were imported into the simulation model (Fig. 10). The York Generator was modeled in CST in full-wave simulations (Fig. 11). The result from measurement and simulation had less than a 4 dB error (typically much less) over the frequency band from 30 to 300 MHz which verified the accuracy of the method.

Next, the impact of variations in the common-mode termination impedance was studied. Although an allowable deviation in the 150 Ω common-mode termination impedance of an imbalanced LISN is reported in [1], [13], and [20] and is qualitatively known, it is also important to quantify the impact of a termination with a nonzero phase. In [13], an acceptable variation of $a \pm 10\%$ change in magnitude and $\pm 30°$ phase change was proposed. An analysis using this variation was performed to demonstrate the risk of such changes in the termination impedance on the radiated emissions from a real setup. Since both the reflection coefficient (18) and emissions (19) are nonlinearly related to the termination parameters, it is problematic to analytically find the worst-case uncertainty from termination variations. The worst case was found using a global random search instead, as follows. Assume the magnitude of the termination impedance is defined as a random variable X_i, where

$$X_i = X_i^{\min} + \left(X_i^{\max} - X_i^{\min}\right) \times \text{rand}(1, N) \tag{20}$$

and the parameter $X_i = \text{unif}(X_i^{\min}, X_i^{\max})$ is a uniformly distributed random number on the interval $(X_i^{\min}, X_i^{\max})$, and *rand*(1, *N*) is the MATLAB function for generating *N* uniformly distributed random numbers. Here, the interval was defined to create a $\pm 10\%$ change in magnitude as specified for this termination, and $N = 2000$ terminations were used in this study. While the true random distribution of impedances may not be uniform, the precise distribution is not critical here since the intent is to find the worst-case uncertainty.

The phase of the termination impedance can similarly be defined as a random variable as

$$Y_i = Y_i^{\min} + \left(Y_i^{\max} - Y_i^{\min}\right) \times \text{rand}(1, N) \tag{21}$$

where the parameter $Y_i = \text{unif}(Y_i^{\min}, Y_i^{\max})$ is a uniformly distributed random number on the interval $(Y_i^{\min}, Y_i^{\max})$. The

[1]Registered trademark.

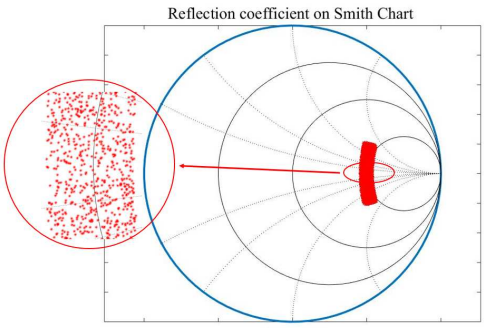

Fig. 12. Reflection coefficients for the one-wire setup associated with random samples of the termination impedance.

interval was set to achieve $a \pm 30°$ variation in phase as specified for this termination. As before, $N = 2000$.

A random termination impedance can be calculated from X_i and Y_i as

$$Z_i = X_i e^{j\frac{\pi}{180}Y_i}. \tag{22}$$

The reflection coefficient for each sample was calculated using (18). The estimated reflection coefficients are plotted on the Smith chart in Fig. 12, where each red dot represents one random sample. The radiated emissions for each random reflection coefficient were found using (19). After calculating the transfer functions from the full-wave simulation, the postprocessing for the 2000 test cases required about 40 min in MATLAB [17]. A full-wave simulation for a single test case, on the other hand, took longer than three hours for the one-wire setup, which clearly illustrates the advantage of the proposed postprocessing method.

The radiated emissions found using (19) associated with all 2000 random terminations of the one-wire setup are shown in Fig. 13. The change in radiated emissions with frequency is caused by resonances in the cable associated with the cable length. The maximum variation in the radiated fields for the random terminations occurs roughly at $f =$ 30 and 180 MHz and is about 2.5 and 2 dB, respectively. Above roughly 250 MHz, the difference is less than 1.5 dB. These results indicate that the termination has the largest effect at lower frequencies (below 250 MHz). For frequencies above 250 MHz, the wavelength is comparable to the length of the cable, so the radiation is dominant at the source region and does not depend substantially on the termination impedance. The maximum variation in the radiation when using the specified tolerance with the one-wire setup is only 2.5 dB and occurs around 30 MHz. This variation in emissions is relatively small and likely acceptable.

B. Two-Wire Setup

The two-wire setup was analyzed with the imbalanced termination connections shown in Fig. 5(a). Equation (7) was verified using the series *RLC* combinations: (port2 replaced by $R_{\mathrm{DM}} = 90\ \Omega$, $L_{\mathrm{DM}} = 10$ nH, $C_{\mathrm{DM}} = 70$ pF) and (port3 replaced by $R_{\mathrm{CM}} = 135\ \Omega$, $L_{\mathrm{CM}} = 10$ nH, $C_{\mathrm{CM}} = 70$ pF). As shown in Fig. 14, the results from the full-wave simulation and from (7) varied by less than 0.4 dB from 30 to 300 MHz.

Here, we assumed the excitation source was 50 Ω. The input reflection coefficient (Γ_1) is zero in this case. It should be noted that any source impedance could be used, but 50 Ω was chosen for convenience since it simplifies the formulations used in this article and since this impedance mimics the York generator. After the approach was validated, it was used to quantify the impact of varying the termination impedances within a specified tolerance.

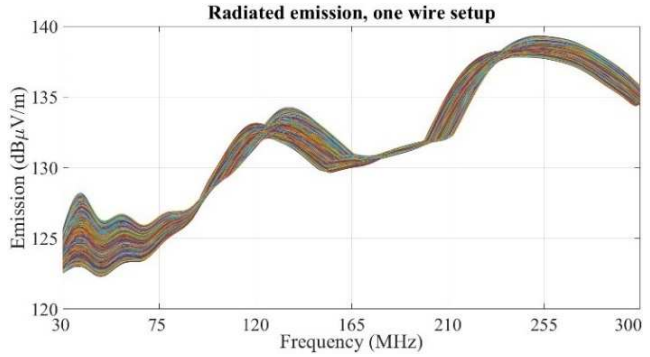

Fig. 13. Radiated emissions (E field) associated with 2000 random terminations varying by ±10% in magnitude and ±30° in phase (one-wire setup).

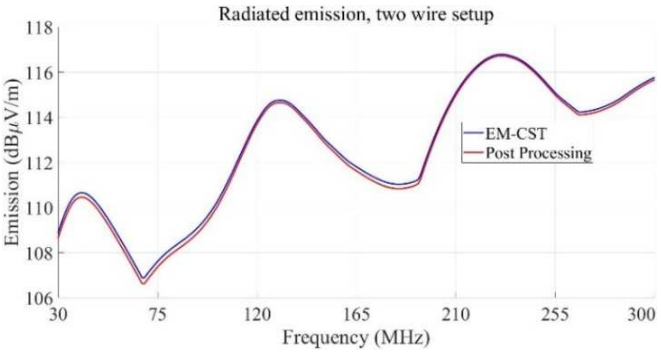

Fig. 14. Comparison of the radiated emissions (E field) found using a full-wave solver and found using (7) for the two-wire setup. The difference is less than 0.4 dB.

A global random search of the maximum radiated emissions from the two-wire setup was performed as with the one-wire setup while allowing the common-mode and differential-mode termination impedances to vary by ±10% in magnitude and ±30° in phase from their ideal values. The reflection coefficients associated with the 2000 random impedances are shown on the Smith chart in Fig. 15. The radiated emissions associated with these terminations were found using (7) and are shown in Fig. 16. This postprocessing step for the 2000 test cases took about 50 min, compared to about 4 h to perform a single full-wave simulation. The radiated emission varies by up to about 4.3 dB from the ideal case across the 30–300 MHz frequency range.

C. Three-Wire Setup

The three-wire setup was analyzed using the imbalanced three-wire termination shown in Fig. 5(c). An analysis was done using both differential-mode excitation [Fig. 5(d)] and tertiary-mode excitation [Fig. 5(e)]. Equation (12) was first verified by terminating the setup with the series *RLC* combinations: (port2 replaced by $R_{\mathrm{DM}} = 90\ \Omega$, $L_{\mathrm{DM}} = 10$ nH, $C_{\mathrm{DM}} =$ 90 pF), (port3 replaced by $R_{\mathrm{TM}} = 50\ \Omega$, $L_{\mathrm{TM}} = 10$ nH, $C_{\mathrm{TM}} =$ 117 pF) and (port4 replaced by $R_{\mathrm{CM}} = 80\ \Omega$, $L_{\mathrm{CM}} = 10$ nH,

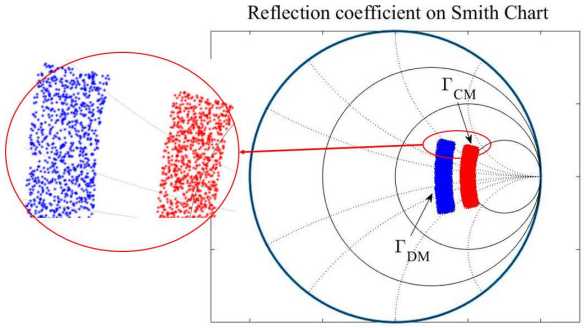

Fig. 15. Reflection coefficients for the two-wire setup associated with random samples of the termination impedance.

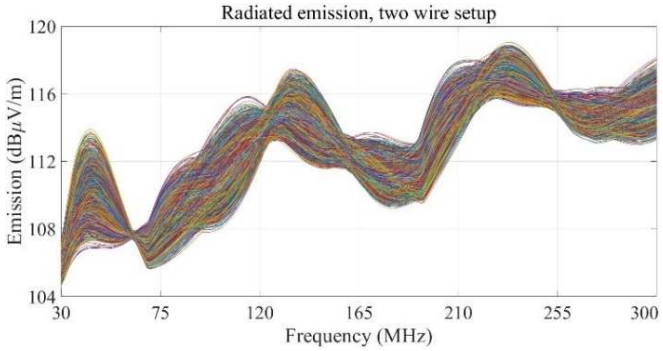

Fig. 16. Radiated emissions (E field) from differential-mode excitation associated with 2000 random terminations varying by ±10% in magnitude and ±30° in phase (two-wire setup).

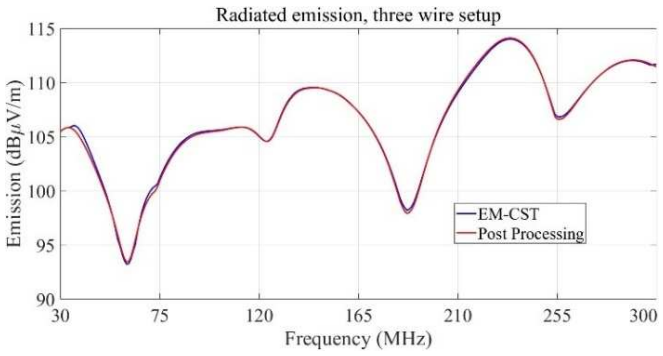

Fig. 17. Radiated emission (E field) from differential-mode excitation (three-wire setup with Error < 0.5 dB).

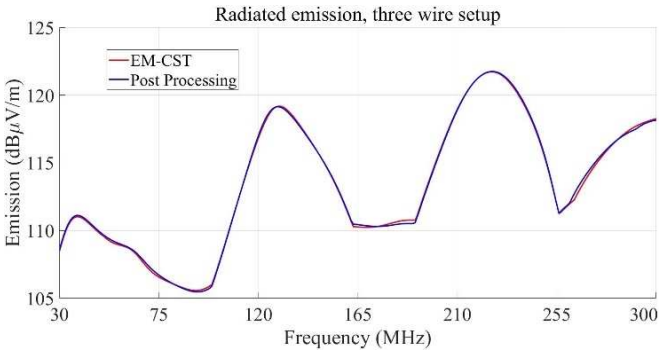

Fig. 18. Radiated emissions (E field) from tertiary-mode excitation (three-wire setup with Error < 0.5 dB).

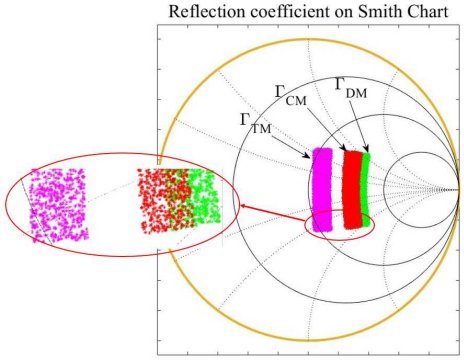

Fig. 19. Reflection coefficients for the three-wire setup associated with random samples of the termination impedance.

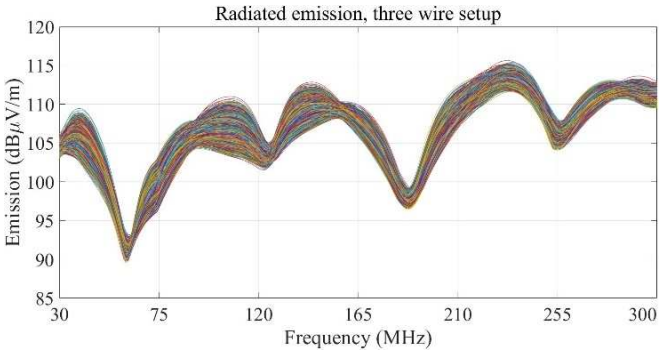

Fig. 20. Radiated emissions (E field) from differential-mode excitation associated with 2000 random terminations varying by ±10% in magnitude and ±30° in phase (three-wire setup).

$C_{CM} = 90$ pF). As shown in Figs. 17 and 18, the results from the full-wave simulation and from (11) varied by less than 0.5 dB from 30 to 300 MHz for the differential-mode excitation and by less than 0.5 dB for the tertiary-mode excitation. The terminations of the three-wire setup were varied randomly to within a 10% tolerance in magnitude and ±30° tolerance in phase. The reflection coefficients for 2000 randomly selected termination impedances are shown in the Smith chart in Fig. 19 for the common-mode, differential-mode, and tertiary-mode excitation.

Radiated emissions for each random termination were estimated using (12), as shown in Fig. 20, for the differential-mode excitation, and in Fig. 21 for the tertiary-mode excitation.

Estimation of the radiated emissions using (12) took about 2.5 h compared to roughly 5 h for a single full-wave simulation of this setup.

The difference between the maximum radiation and the ideal case for the differential-mode excitation (shown in Fig. 20) is less than 5.5 dB and is less than 3.3 dB for the tertiary-mode excitation (Fig. 21).

IV. Impact of Termination Condition on Measurement Uncertainty

The CISPR 16-4-1 standard [14] specifies the level of uncertainty that is allowed in radiated emissions tests. Uncertainties addressed include the cable terminating conditions, as well as variations due to the cable arrangement, EUT operating condition, and measurement instrumentation. The calculations in Section IV were made to ensure the uncertainty caused by the specified tolerance in imbalanced termination impedances will meet the goals of the standard.

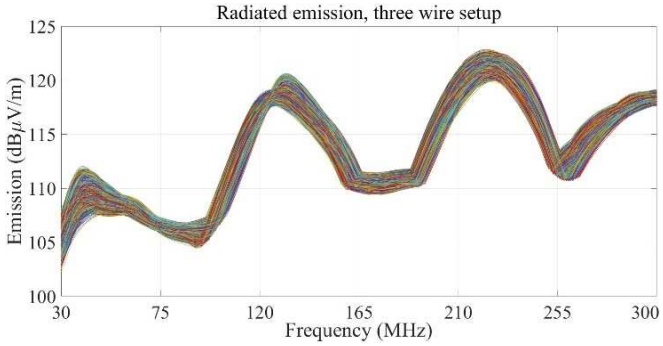

Fig. 21. Radiated emissions (E field) from tertiary-mode excitation associated with 2000 random terminations varying by ±10% in magnitude and ±30° in phase (three-wire setup).

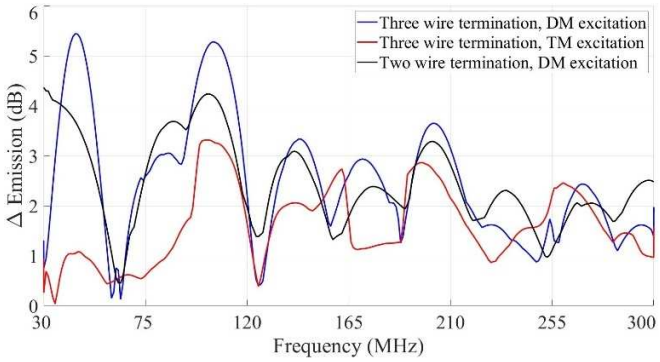

Fig. 22. Maximum change in radiated emission (E field) due to simulated variations in the terminating conditions for the two and three-wire setup.

The average combined standard uncertainty, $U_{\text{c-scu}}$, is defined by the standard as [9]

$$U_{\text{c-scu}} = \sqrt{U_{\text{c-MIU}}^2 + U_a^2 + U_b^2 + U_c^2} \tag{23}$$

where $U_{\text{c-MIU}}$ is the combined measurement instrumentation uncertainty and is specified in CISPR/TR 16-4-1 to be no more than 2.5 dB, U_a is the uncertainty from the main cable arrangement and should be no more than 3.5 dB, U_c is the uncertainty in the EUT operating condition and should be no more than 1.7 dB, and U_b is the uncertainty in terminating conditions. The expanded standard uncertainty, U_{scu}, defines an interval within which the measurement can confidently be asserted to lie, and is given by [9], [25], and [26]

$$U_{\text{scu}} = 2U_{\text{c-scu}}. \tag{24}$$

CISPR 16-4-1 suggests this uncertainty should be limited to 15.5 dB [14].

Assuming the cable terminating conditions vary with a rectangular probability distribution (as is done in this article), the uncertainty caused by the terminating condition U_b is given by [9] and [14]

$$U_b = \frac{E_{\max} - E_{\min}}{2\sqrt{3}} = \frac{\Delta E}{2\sqrt{3}} \tag{25}$$

where $E_{\max}$ and $E_{\min}$ are the maximum and minimum electric field strength in dBμV/m, respectively, caused by variations in the terminating conditions.

Fig. 22 shows the maximum deviation in the radiated emissions [i.e., $E_{\max}$–$E_{\min}$ as in (25)] when using differential-mode and tertiary-mode excitations in the two-wire and three-wire setups and while varying the imbalanced termination impedances within the ±10% deviation in magnitude tolerance and ±30° deviation in phase tolerance. The maximum change in emissions among all test cases for the defined tolerance in termination impedance is about 5.5 dB. The maximum deviation occurs around 40 MHz in the three-wire setup with a differential-mode excitation. This is about 6.5 dB lower than the 12 dB of uncertainty reported for a balanced three-wire VHF-LISN termination in [9]. In [9], the PE wire is connected to the enclosure in a balanced termination; thus, the common-mode impedance is low for all currents. For the imbalanced three-wire termination, however, the PE is not grounded, so this termination may suppress resonances more strongly than the balanced termination, resulting in a lower measurement uncertainty [13].

Because the maximum deviation in radiated emissions due to the variation in termination impedance of the imbalanced two-wire and three-wire setups was about 5.5 dB, the maximum uncertainty in terminating condition (U_b) from (25) is about 1.6 dB.

Using (23) with the maximum allowed variations in uncertainty for the other parameters, the average combined standard uncertainty for the terminating condition (Uc-scu) for two and three wires would be about 4.9 dB, and the expanded standard uncertainty (USCU) would be about 9.8 dB for an imbalanced two or three-wire termination with the specified tolerances. According to the model used in this article, the uncertainty from a two-wire or three-wire imbalanced LISN is below the suggested CISPR 16-4-1 15.5 dB limit and is lower than the 12 dB USCU, VHF LISN uncertainty reported in [9] for a balanced LISN.

V. Conclusion

VHF LISNs are used to reduce measurement uncertainty in radiated emissions tests. While balanced LISNs are used in most standardized testing, balanced terminations are rarely available in practice. An imbalanced LISN gives a better assessment of the worst-case emissions that may be encountered in the real world. Defining acceptable tolerances in the common-mode terminations seen within these imbalanced LISNs is important to standardize their application.

In this article, a postprocessing method was implemented to investigate the effects that variations in the complex termination of imbalanced LISNs will have on radiated emissions, in particular, terminations within the ±10% tolerance in magnitude and ±30° tolerance in phase specified in [11] and [13]. The postprocessing method was used to reduce the number of full-wave simulations and make a parametric sweep of the possible complex termination impedances. The equivalent S-parameters between termination ports and the radiated field were used to develop formulas that determine the radiated emissions in terms of the source currents and the termination impedances (which were represented as reflection coefficients). As a result, it is possible to perform a full-wave simulation once to calculate the transfer functions and then rapidly estimate the radiated emissions for a wide variety of complex termination impedances using only the formulas.

Test cases using a one-wire, imbalanced two-wire, and three-wire setup were used to validate the postprocessing

approach and to investigate the impact of allowable deviations in the cable terminations. Comparisons between radiated emissions predicted by the postprocessing method and emissions found using full-wave simulations found less than a 1 dB difference in the maximum predicted field between the two approaches for the three setups studied, validating the simulation methodology. The postprocessing approach, however, was substantially faster than using full-wave simulations. Predicting the radiated emissions from 2000 terminations took from 40 to 60 min for the one-wire, two-wire, and three-wire setups using the proposed postprocessing approach, while a single full-wave simulation with a given set of termination impedances took from 3 to 5 h. We expect similar simulation times to be observed for other DUT configurations.

Results show that variations in the termination impedance have the largest impact on radiated emissions at lower frequencies. For the cases studied here, the variations in radiated emissions were minimal above 400 MHz when the length of the cable became comparable to a wavelength. When the cable becomes electrically long, the attenuation from radiation becomes more important than the termination, as resonances are suppressed, and less power reaches the termination.

The postprocessing approach was used to estimate radiated emissions while varying the imbalanced termination impedances by $\pm 10\%$ in magnitude and $\pm 30^\circ$ in phase for the 2- and 3-wire setups. The maximum variation in the observed electric fields (i.e., $E_{\max} - E_{\min}$) for the setups studied here was 4.5 dB for the 2-wire setup and 5.5 dB for the 3-wire setup. As a result, the maximum expanded standard uncertainty for the two setups was 9.8 dB. This uncertainty is well below the 15.5 dB suggested by CISPR 16-4-1, suggesting that these tolerances should be acceptable for standardized EMC measurements using imbalanced LISNs. It should be noted that variation in cable configuration, EUT height, size, etc., was not considered here and should be considered in a future study.

REFERENCES

[1] S. Okuyama, N. Kuwabara, K. Osabe, and H. Muramatsu, "Improvement of radiated emission measurement reproducibility with VHF-LISN obtained from final results of international inter-laboratory comparison on termination control of power line," in *Proc. Asia–Pacific Symp. Electromagn. Compat. (APEMC)*, May 2015, pp. 589–592.

[2] C. Miyazaki, K. Tanakajima, M. Yamaguchi, S. Satake, and J. Kawano, "Improvement of dispersion of radiated emission measurement results by VHF-LISN," in *Proc. IEEE Int. Symp. Electromagn. Compat.*, Aug. 2008, pp. 1–4.

[3] S. Okuyama, N. Kuwabara, K. Osabe, and H. Muramatsu, "Influence of disturbance current mode on correlation between radiation test sites using VHF–LISN and CMAD," in *Proc. Int. Symp. Electromagn. Compat. (EMC EUROPE)*, Amsterdam, The Netherlands, Aug. 2018, pp. 494–499.

[4] C. Miyazaki, K. Tanakajima, M. Yamaguchi, K. Endo, H. Muramatsu, and J. Kawano, "A round-robin test on effectiveness of a VHF LISN for radiated emission measurements," in *Proc. IEEE Int. Symp. Electromagn. Compat.*, Aug. 2011, pp. 405–410.

[5] S. Okuyama, K. Osabe, K. Tanakajima, and H. Muramatsu, "Investigation on effectiveness of very high frequency line impedance stabilization network (VHF-LISN) for measurement reproducibility," in *Proc. Int. Symp. Electromagn. Compat.*, Brugge, Belgium, Sep. 2013, pp. 174–179.

[6] K. Osabe, N. Kuwabara, and S. Okuyama, "Termination impedance for AC mains cable leaving from EUT area in radiated emission measurement," in *Proc. Int. Symp. Electromagn. Compat.-EMC Eur.*, Angers, France, Sep. 2017, pp. 1–6.

[7] S. Okuyama, N. Kuwabara, M. Yamaguchi, and K. Osabe, "Improvement in the reproducibility of radiated emission measurements in a fully anechoic room by using VHF-LISN to control the termination condition of the AC mains cable leaving the EUT," in *Proc. Asia–Pacific Int. Symp. Electromagn. Compat. (APEMC)*, vol. 1, May 2016, pp. 50–52.

[8] Y.-C. Tang, J.-S. Chen, C.-H. Lee, and C.-N. Chiu, "A case study on the consistency improvement in radiated-emission testing by using LISN," in *Proc. Int. Symp. Electromagn. Compat., Tokyo*, May 2014, pp. 259–262.

[9] K. Osabe, N. Kuwabara, and H. Muramatsu, "Impacts to measurement uncertainty of radiated EMI measurement by setting terminating condition of AC mains cable leaving from test area," in *Proc. IEEE Int. Symp. Electromagn. Compat. IEEE Asia–Pacific Symp. Electromagn. Compat. (EMC/APEMC)*, May 2018, pp. 52–56.

[10] "Artificial Mains Networks for the boundary of the EMC test volume," Int. Electrotechnical Commision (IEC), Geneva, Switzerland, Tech. Rep. CISPR Working Group 2, Aug. 2017.

[11] K. Osabe, N. Kuwabara, and H. Muramatsu, "Justification of balanced VHF-LISN termination," in *Proc. EMC Symp.*, Spokane, WA, USA, Aug. 2022, p. 604.

[12] D. M. Lauder and R. C. Marshall, "Measurement uncertainty and cable balance–with implications for the CDNE-M and CMAD," in *Proc. Int. Symp. Electromagn. Compat.*, Sep. 2014, pp. 801–806.

[13] H. Rezaei, M. Sørensen, W. Huang, D. G. Beetner, and D. Pommerenke, "Analyzing the influence of imbalanced Two- or three-wire VHF LISN on radiated emissions from AC cables," *IEEE Trans. Electromagn. Compat.*, vol. 64, no. 2, pp. 327–337, Apr. 2022.

[14] "Specifications for radio disturbance and immunity measuring apparatus and method- part 4–1: Uncertainties, statistics and limit modelling—Uncertainties in standardized EMC tests," Int. Electrotechnical Commision (IEC), Geneva, Switzerland, Tech. Rep. CISPR/TR 16-4-1, Feb. 2009.

[15] H. Rezaei, "Source reconstruction in near field scanning for RFI application," Doctoral dissertation, Dept. Elect. Comput. Eng., Missouri Univ. Sci. Technol., Rolla, MO, USA, 2021.

[16] *Dassault Systèmes*. Accessed: 2024. [Online]. Available: https://www.3ds.com

[17] [Online]. Available: https://www.MATLAB.com

[18] C. A. Balanis, *Antenna Theory: Analysis and Design*. Hoboken, NJ, USA: Wiley, 2016.

[19] S. J. Mason, "Feedback theory—Some properties of signal flow graphs," *Proc. IRE*, vol. 41, no. 9, pp. 1144–1156, Sep. 1953.

[20] *Characteristics of the Asymmetric Artificial Network*, CISPR, Geneva, Switzerland, 2019.

[21] S. B. Worm, "On the relation between radiated and conducted RF emission tests," in *Proc. 13th Int., Zurich Symp. Tech. Exhibit. EMC*, Feb. 1999, pp. 515–520.

[22] M. J. Coenen, "Common mode impedance measurements on cables in the frequency range 30 MHz-1 GHz," Philips Semiconductors, Tech. Rep. EIE 92004, 1992.

[23] *York (CNE) Comparison Noise Emitter. 30 MHz—1 GHz*. Accessed: 2024. [Online]. Available: https://www.emchire.co.uk/

[24] *R&S ZNB4 VNA*. Accessed: 2024. [Online]. Available: https://www.rohde-schwarz.com/us/products/test-and-measurement/network-analyzers/rs-znb-vector-network-analyzer_63493-11648.html

[25] "Information technology equipment—Radio disturbance characteristics—Limits and methods of measurement," Int. Electrotechnical Commission (IEC), Geneva, Switzerland, Tech. Rep. CISPR 22, 2006.

[26] D. A. Hill and M. Kanda, "Measurement uncertainty of radiated emissions," NIST, Tech. Rep. 1389, 1389.

Hossein Rezaei (Member, IEEE) received the B.S. degree in electrical engineering from Islamic Azad University Najafabad Branch (IAUN), Najafabad, Iran, in 2004, the M.S. degree in electrical engineering from Shiraz University of Technology, (SUTech), Shiraz, Iran, in 2011, and the Ph.D. degree in electrical engineering from the EMC Laboratory, Missouri University of Science and Technology, Rolla, MO, USA, in 2021.

From 2020 to 2021, he worked with ESDEMC Technology LLC, Rolla, on developing ESD testing solutions. In March 2021, he joined Intel, Folsom, CA, USA. In January 2022, he joined Solidigm Technology, Rancho Cordova, CA, USA. His research interests include electromagnetic discharge modeling and analysis, electromagnetic compatibility, signal integrity, RF desense, and numerical simulations.

Morten Sørensen (Senior Member, IEEE) received the M.S. degree in physics from Aarhus University, Aarhus, Denmark, in 2005, and the Ph.D. degree in electrical engineering from Aalborg University, Aalborg, Denmark, in 2018.

From 2006 to 2017, he was an EMC and Antenna Specialist with Bang & Olufsen, Struer, Denmark, including three years, from 2011 to 2014, as a Researcher and the Technical Project Manager with the Innovation Consortium, "EMC Design—First Time Right." From 2017 to 2019, he was a Visiting Assistant Research Professor with the EMC Laboratory, Missouri University of Science and Technology, Rolla, MO, USA. From 2019 to 2022, he was an Associate Professor with the Centre for Industrial Electronics, University of Southern Denmark, Odense, Denmark. Since 2022, he has been a Senior Specialist with FORCE Technology, Aarhus, Denmark, and a Danish Research and Technology Organization. His current research interests include near-field scanning, RF designs, electrostatic discharge, and system-level radiated emission.

Kim Jensen (Member, IEEE) received the degree in electronic engineer from Aarhus, Viby, Denmark, 1987.

He is currently with Grundfos, Bjerringbro, Denmark, where he is the Chief EMC Specialist with the EMC Laboratory, a part of the Global Laboratory. He was an EMC Specialist at Ericsson, Struer, Denmark, from 1988 to 2010, working with telecommunication network equipment, and Senior EMC Specialist at Bang & Olufsen, Struer, from 2010 to 2015, working with audio and video equipment, including radio approval procedures. He was a member of the Innovation Consortium "EMC—First Time Right" in Denmark (2010–2013), working with the influence of variations in common-mode termination impedances on radiated emissions.

David Pommerenke (Fellow, IEEE) received the Diploma and Ph.D. degrees in electrical engineering from Technical University Berlin, Berlin, Germany, in 1990 and 1996, respectively.

He was with EMC, Hewlett Packard, Roseville, CA, USA, for five years, and joined as a Faculty Member with the Electromagnetic Compatibility Laboratory, Missouri University of Science and Technology, Rolla, MO, USA. In 2020, he also joined as a Faculty Member with the Graz EMC Laboratory, Graz University of Technology, Graz, Austria. His current research interests include system-level ESD, electronics, numerical simulation, EMC, measurement methods, and instrumentation.

Dr. Pommerenke is an Associate Editor of IEEE TRANSACTIONS ON ELECTROMAGNETIC COMPATIBILITY.

Daryl G. Beetner (Fellow, IEEE) received the B.S. degree in electrical engineering from Southern Illinois University, Edwardsville, IL, USA, in 1990, and the M.S. and D.Sc. degrees in electrical engineering from Washington University, St. Louis, MO, USA, in 1994 and 1997, respectively.

He is with Missouri University of Science and Technology (Missouri S&T), Rolla, MO, USA, where he is currently a Professor of electrical and computer engineering, the Director of the Electromagnetic Compatibility Laboratory, Missouri S&T, and the Director of the Center for Electromagnetic Compatibility, National Science Foundation Industry/University Cooperative Research Center.

Dr. Beetner was the 2020 recipient of the IEEE EMC Society Technical Achievement Award and the 2003 IEEE-HKN C. Holmes MacDonald Outstanding Young Electrical Engineering Professor. He has received a number of best paper awards, including honorable mention for the Richard B. Schulz Best Transaction Paper award. He currently serves the IEEE EMC Society as a member of the EMCS Board of Directors, the Chair for the TC-4 Electromagnetic Interference Control, the EMC Education Grants Chair, and the IEEE Medal for Environmental and Safety Technologies Selection Committee, and a member of the IEEE Medals Council and the IEEE-HKN Outstanding Young Professional Committee.